Cleat Traction Tester

Alexandra Lee and Remi Sandell

2.70 FUNdamentals of Precision Machine Design
Alexander Slocum

1. Introduction

The biomechanics of lower extremity injuries have been a focus of study in sports medicine. In particular, ACL tears stand out due to their high incidence rates, extensive recovery periods, and long-term effects on athletes' careers and quality of life. In cleated sports such as soccer and football, these injuries often result from interactions between an athlete's footwear and the playing surface. Cleats designed to optimize traction can unintentionally introduce high rotational forces that place stress on the knee and increase the risk of injury (Fong et al., 2011).

Researchers and designers must understand how cleats interact with various playing surfaces under realistic conditions to mitigate this risk of injury. By simulating the forces and motions during athletic maneuvers, engineers can test cleat designs to increase performance and safety.

A traction testing device that measured translational and rotational force was created to address this need. The first iteration of a Cleat Traction Tester successfully measured critical parameters to gather insights into the relationship between cleat designs, playing surfaces, and injury mechanisms. However, practical limitations, including restricted range of motion, reliance on external power systems, and lack of modularity, highlighted the need for further improvement.

This paper presents a second iteration of the Cleat Traction Tester and builds on the original design's foundation while addressing its shortcomings. By using mechanical features and a more portable, modular design, the new iteration provides a more robust and accessible cleat testing solution.

2. Background

2.1 ACL Injuries

The anterior cruciate ligament (ACL) is a critical stabilizing structure in the knee joint that resists anterior translation and rotational forces. ACL tears are among the most severe lower-extremity injuries in sports because of their long recovery periods, potential for chronic instability, and risks of early-onset osteoarthritis. These injuries occur when forces exceed the ligament's tensile capacity, but approximately 70% of ACL injuries are non-contact in nature (Griffin et al., 2000, Boden et al., 2000, Meyer and Haut, 2008). This means an athlete's own movements are interacting with the environment to create these damaging loads on the knee.

2.2 ACL Injury Risk Factors

ACL injuries can stem from a combination of biomechanical, anatomical, and environmental factors that stress the ligament.

Biomechanically, athletic maneuvers significantly affect ACL injury risk. Cutting, landing, and pivoting movements create loading conditions with varying normal and rotational forces. Normal forces are from the athlete's body weight and momentum and rotational forces are generated when the foot is planted and the body rotates (Livesay et al., 2006). For example, the "knee-in, toe-out" position is particularly hazardous because it creates an alignment that

shifts the load from the muscle structures to the ligament, overloading the ACL. As a result, there is an inward load on the knee, inward rotation of the tibia, and shear forces (Fong et al., 2011, Griffin et al. 2006).

Females are four to six times more likely to experience ACL injuries than males due to several potential differences (Hewett et al., 2005). In general, the wider pelvis in females increases the angle range for the quadriceps and for valgus knee alignment, a narrower space through which the ACL passes can increase the likelihood of ligament damage, and even fluctuations in hormone levels may alter ligament tensile strength (Griffin et al. 2006). However, a high rate of non-contact injuries suggests shortcomings in footwear design, where a significant gender gap also exists (Boden et al., 2000).

The relationship between footwear design and playing surfaces can play a critical role in ACL injuries. High linear traction allows players to accelerate and decelerate effectively, but excessive rotational traction can increase knee torque and ACL injury risk (Livesay et al., 2006). A challenge in current footwear design is that these cleat-surface interactions change with the environment. Harder surfaces like artificial turf reduce the deformation of cleats, leading to higher rotational traction, whereas wet or muddy fields reduce overall traction. Dry and well-maintained fields also promote high traction forces, which are good for linear performance but can elevate injury risks during cutting and pivoting (Orchard, 2001).

2.3 Cleat Design

Cleat footwear brands have experimented with a variety of cleat designs because stud length, arrangement, and material stiffness directly influence traction properties. For example, circular studs allow more freedom of rotation, while bladed studs are designed for maximum linear grip but increase the potential for dangerous knee torques (Livesay et al., 2006). Ideal cleat designs to mitigate ACL injury risk must be designed to provide sufficient linear traction for performance yet limit rotational traction to prevent excessive torques on the knee. To find optimal configurations and materials for cleats, it is important to test and gather data on these designs under realistic conditions.

2.4 Cleat Traction and Torque Tester

The initial Cleat Traction Tester was developed to measure the translational and rotational traction forces exerted by soccer cleats. This design aimed to replicate the biomechanical forces experienced during cutting and pivoting motions to evaluate the performance and safety characteristics of cleated footwear.

The device used a central circular bearing for rotational motion and leg angles, a hydraulic system to create a simulated vertical force applied during a cutting movement, a base plate that a cleat could be mounted to that mimicked various field surfaces, and a force measurement system to gather quantitative data on translational and rotational forces exerted during tests.

While the first iteration of the Cleat Traction Tester successfully demonstrated the feasibility of measuring cleat traction forces, it had several practical limitations that restricted its usability and effectiveness.

The circular bearing system restricted the range of leg angles that could be simulated and prevented tests mimicking the more extreme movements that might be seen in a competitive game and during ACL injury. The reliance on these complex bearings, force sensors, and other high-end components also made the system relatively expensive. This hinders its potential for adoption, particularly for iterative prototyping or use by smaller organizations.

The device relied on a continuous connection to an external power and air supply to generate air pressure for normal force loading. The design was also not modular, making it bulky to transport, so different test conditions and field surfaces were not accessible. These dependencies reduced the portability of the system and made it impractical for field testing. This meant that while the device could simulate forces under controlled conditions, its applicability to real-world scenarios was limited.

These shortcomings highlighted the need for a second iteration that would provide a greater range of simulated leg angels, lower costs, reduce dependency on external systems, and improve modularity to enable portable and field-ready testing. The initial cleat traction tester laid the foundation for advancing cleat evaluation. Its design has provided insights that guide the development of a second iteration aimed at overcoming these challenges and expanding its functionality.

3. Functional Requirements

3.1 Design Requirements

Following the 'FREDPARRC' framework (Slocum, 2008), the design requirements for the next iteration of the Cleat Traction Tester are described below.

1. **Simulation of Realistic Loading Conditions:** The system must apply a normal vertical force of up to 2000 N at different angles, simulating the typical dynamic loads exerted by athletes. The load application system must maintain consistent force application throughout testing. It should also be a system that does not rely on high amounts of external power or air supply.
2. **Accurate Application and Measurement of Rotational and Linear Traction Force:** The system must apply and measure rotational torques of up to 10 Nm and linear traction forces of up to 100 N. The rotational torque should be applied to the center of pressure of a soccer cleat or cleat sole.
3. **Increased Range of Simulated Angles:** To test different leg angles, the device must allow for at least 45º of motion in every direction. This allows for better mimicking of cutting and pivoting motions.
4. **Accommodates Various Cleats:** The cleat attachment must accommodate cleats of varying sizes, ranging from a women's size 4 (20.8cm) to men's size 16 (32.1cm). It must

hold the cleat in place without altering its interaction with the testing surface, and allow for torque measurements at different centers of pressure during athletic movements.

5. **Adaptable to Various Playing Surfaces:** The device should be able to perform field testing on a variety of playing surfaces.
6. **Portable and Lightweight Design:** A single user must be able to transport the device.

3.2 Overview of Physics Applied

The second iteration of the Cleat Traction Tester must accurately simulate and measure forces exerted during athletic movements, including cutting and pivoting. The physics include a normal force of 2000N, a rotational torque of 10 Nm, and a horizontal traction force of 100N.

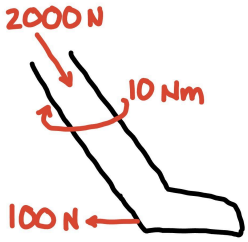

Figure 1: General physics of the problem that must be replicated in our Cleat Traction Tester design.

The test device must replicate these forces while maintaining structural integrity and providing precise measurements.

3.3 Risks and Countermeasures

The design and development of the second iteration of the Cleat Traction Tester involves addressing potential risks to ensure functionality, portability, and accuracy.

First, the requirement for high loading forces may increase system size, leading to a bulky and heavy device that is difficult to use in the field. We can design the device to be modular for easier storage and select a more lightweight yet durable material. This way, the device can still be easily stored and transported.

Variability in shoe sizes may affect locations where the tester applies forces and impact measurement accuracy and consistency among sizes. Because of this, the mounted cleat plate should have a variety of mounting points for different centers of pressure. We can also design multiple footplate attachments for the different shoe sizes that can be swapped based on the cleat size and shape.

Differences in the rate of force applications could affect the accuracy of measurements and fail to replicate realistic athletic conditions. For example, slowly increasing a force to reach a value versus quickly applying that force might yield different results. We will address this through a sub-study during the design phase to test different loading rates to ensure that the selected approach on the Cleat Traction Tester can perform consistently.

Failure of components in device design is always a risk. System components such as bearings, force application mechanisms, or frames may fail under repeated application of high forces. Our design process included detailed stress analysis to guide component selection to ensure our degvice withstand repeated loading without failure.

4. Design

4.1 Overall Cleat Traction Tester Design

Based on our design requirements, we created the second iteration of the Cleat Traction Tester, as shown in Figure 2. The vertical normal force is applied via a lead screw that compresses a spring, the horizontal force is applied via a rope that goes over a pulley, and the torque is applied by a torque wrench that attaches to a rod connected to the footplate at the center of pressure. The device is grounded to the field using three people of greater than 150 lbs each standing on the platforms. The different modules can be either easily taken apart or folded up, allowing the device to be portable. In addition, it is a purely mechanical device that does not require any power or air source to function. This allows it to be used on any playing field.

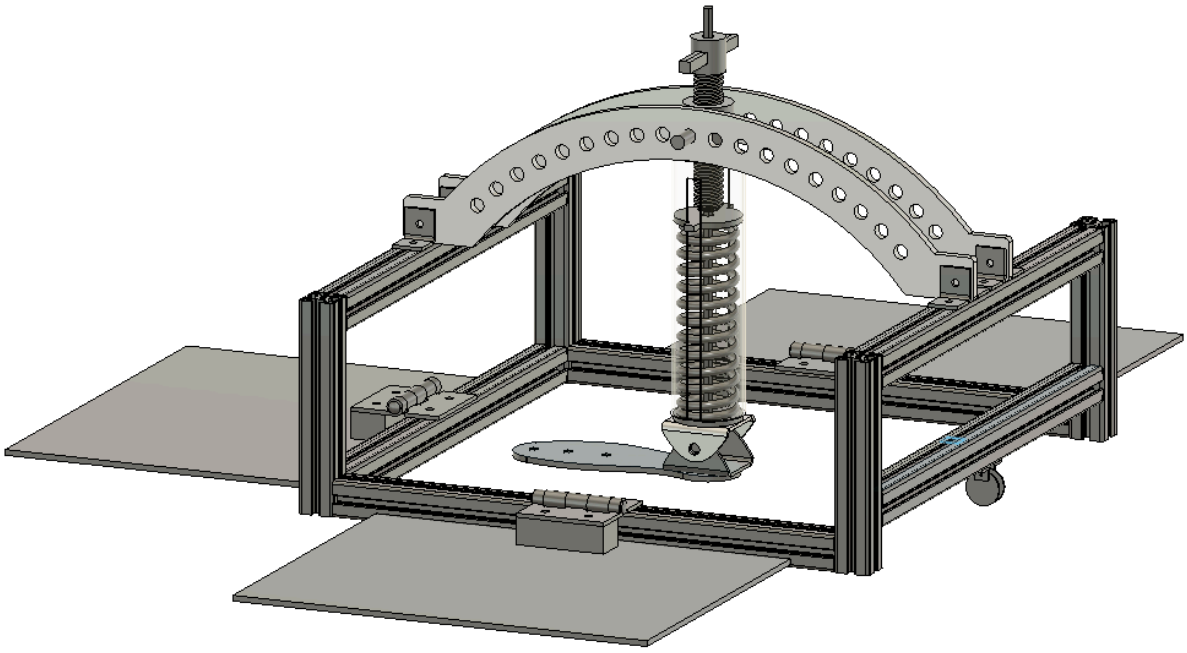

Figure 2: CAD model of the entire system.

4.2 Vertical Force Module

The vertical force module in figure 3 is a critical component of the Cleat Traction Tester, designed to replicate the normal forces experienced during athletic movements such as cutting and pivoting. It applies a controlled vertical load of up to 2000 N to the center of pressure, simulating the forces generated by an athlete during gameplay.

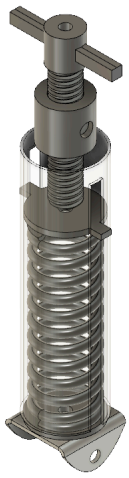

Figure 3: Vertical force module.

The leadscrew is manually turned using a handle to compress a spring, which applies the vertical force. The leadscrew nut is fixed to the frame to provide a “ground” for the system. We chose a leadscrew with a 6.35 mm lead and a diameter of 31.75 mm, and a spring with a spring constant of 230 lb/in. These choices were based on our system analysis.

In choosing a leadscrew and spring system, we wanted to choose a lead that ensured the leadscrew did not require an unreasonable amount of torque for the user to apply. The torque-to-force relationship was determined by (1):

$$T = F \cdot \left(\frac{l}{2\pi} + \mu \cdot \frac{d_m}{2} \right)$$

Where T is the torque required, F is the applied load of 2000 N, l is the lead of the screw, mu is the coefficient of friction, and d_m is the mead diameter of the thread. Our calculated torque was 11.54 Nm, which is a manageable range for manual operation.

We wanted to ensure the leadscrew would not buckle under the maximum applied force. We used Euler’s buckling equation (2):

$$F_{\text{critical}} = \frac{\pi^2 EI}{(KL)^2}$$

Where E was the Young’s Modulus of the steel leadscrew at 200 GPa, I was the moment of inertial of the leadscrew cross-section, k was 2 in the condition of one free and one fixed end, and L was the length of the leadscrew. Even though the leadscrew has support when it interacts with the nut, we used the entire length of the leadscrew in our calculations for a conservative estimate. The calculated load for buckling was about 1.6 x 10^6 N, far exceeding the 2000 N of loading force and ensuring the leadscrew would not buckle.

To keep the leadscrew in a fixed position after loading, the leadscrew was designed to be non-backdrivable. This ensures the spring remains compressed without external locking mechanisms. We used the following equation (3):

$$p < \frac{2\pi r \mu}{\cos\alpha}$$

Where p is the lead, r is the radius of the lead screw, mu is the friction coefficient, and alpha is the thread angle. If the lead is smaller, the lead screw is not backdrivable. This was true in our selection.

The next part of our selection had to relate an appropriate spring to our leadscrew. One of the parameters we needed to consider was the number or turns until full compression or normal force application. This was calculated using (4):

$$\text{Number of Turns} = \frac{\text{Compression Distance}}{\text{Lead}}$$

For safety reasons, the compression distance should be less than two inches, so that the spring has a smaller jumping distance when released. With a human loading torque of an estimated 8 Nm, we were able to find the required spring constant, k, for our system (5):

$$K = \frac{\gamma}{X\left(\frac{L}{2\pi} + \frac{\mu d_m}{2}\right)}$$

We also performed an analysis on the maximum stress on the leadscrew to find the number of cycles it could withstand before fatigue. We used S-N curve for our material, steel, to find that the leadscrew could withstand well over 10^9 cycles.

The carefully chosen components of the vertical force module ensures a efficient application of vertical load that fits our functional requirements.

4.3 Vertical Force Module to Angular Motion Bar Coupling

The coupling of the verical force module to the angular motion bar consists of pins fixed to the nut that interface with the angular motion bars discussed later in the paper. These pins serve as the connection to “ground” for the nut. They allow the nut to freely rotate while restricting translational movement, similar to a knee joint. As a result, the pins must be strong enough to withstand the applied vertical load of 2000 N without yielding or failing under fatigue. Through the following analysis, we chose a shaft with a 15.88 mm (5/8 inch) diameter.

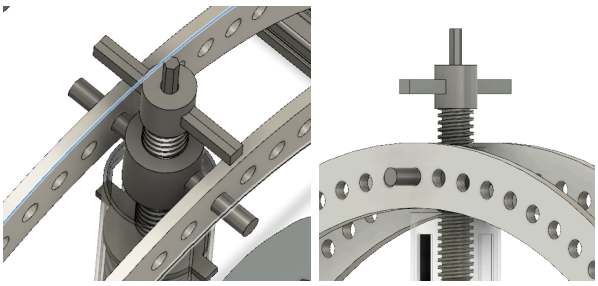

Figure 4: Vertical force coupling to the angular motion bar.

As seen in figure 5, the pins were modeled together with the nut as straight beam with a central load of 2000 N.

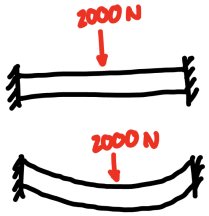

Figure 5: Straight beam bending modeling of pins.

This conservative model assumes that the entire load is applied at the midpoint of the beam. We calculated the maximum stress (6):

$$\sigma_{max} = \frac{M_{max} D}{2I}$$

$$M_{max} = \frac{FL}{4} \quad I = \frac{\pi D^4}{64}$$

So

$$\sigma_{max} = \frac{FLD}{8I}$$

$$\sigma_{max} = \frac{FLD64}{8\pi D^4} = \frac{8FL}{\pi D^3}$$

With F being the applied load of 2000 N, L being the total length from the end of one pin to the end of another, and D being the diameter of the pin, we calculated a maximum stress of 152.6 MPa, which was below the yield strength of the pin material, aluminum, at 240 MPa. This ensured that the pins would not yield under loading, with a safety factor of 2.18.

Our chosen shaft diameter will likely increase in the next iteration of our design because the safety factor of 2.18 should be increased. Because this is such a critical structure that holds a high loaded component in place, the failure of this component is dangerous. By increasing the diameter to 19.05 mm (3/4 inches), the safety factor increases to 3.8, which may be better because of the hazardous failure implications.

The pins are subjected to cyclic loading during repeated operations of the cleat traction tester. To evaluate fatigue, the number of cycles before failure was calculated using the S-N curve for the chosen material, aluminum. The pins were estimated to withstand over 10^9 cycles before fatigue failure.

The coupling between the vertical force module and angular motion bar ensures the stability of the nut while allowing rotational motion critical for cleat testing. It holds the critical vertical force module in place and is a small, but significant component of our design.

4.4 Ankle Joint

The ankle joint module provides rotational freedom to emulate the natural motion of an ankle and allows the footplate to rotate in response to adjustments in the angular motion bars.

The ankle joint consists of two pins, each supporting half of the vertical load, that needs to be designed withstand the applied forces without yielding.

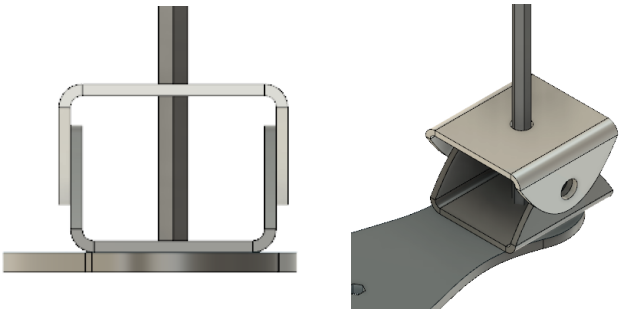

Figure 6: Ankle joint module.

With the vertical load of 2000 N being distributed between the two pins, each pin experiences a force of 1000 N. We can model the pins as cantilever beams with a concentrated load the the free end.

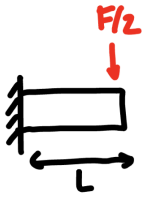

Figure 7: Pin modeled as a cantilever beam where L is the length of the pin and F is the vertical force of 2000 N.

We can find the maximum moment on the beam which is felt at the fixed end, and use that maximum moment to calculate the maximum bending stress on the beam (7).

$$\sigma_{max} = \frac{M_{max} D}{2I}$$

$$M_{max} = \frac{FL}{2} \quad I = \frac{\pi D^4}{64}$$

$$\sigma_{max} = \frac{FLD}{4I} = \frac{FLD64}{4\pi D^4} = \frac{16FL}{\pi D^3}$$

With our selected pin diameter of 12.7 mm (1/2 inch), we calculate a maximum stress of 62.2 MPa. This is well below the yield strength of the pin material of 240 MPa with a safety factor of 3.9. Having a high safety factor helps ensure that unequal load distribution due to tolerances and errors between the two pins do not cause premature failure. We also checked for fatigue using S-N curves, we see that the number of cycles before fatigue is greater than 10^9 cycles, making our pin diameter choice a sound decision.

In manufacturing, we will have to ensure that the pins still have rotation freedom while still holding the footplate in place. We will likely use bushings to aid in this. Through this analysis, the ankle joint module is designed to handle the applied forces.

4.5 Foot Plate Module

The foot plate module serves as the primary interface between the cleat and field surface. It plays a crucial role in transmitting the torque during traction testing. As outlined in the design requirements, the foot plate must accommodate cleats of various sizes, allow for testing different centers of pressure, and withstand the applied rotational torque of 10 Nm without failure.

Figure 8: Foot plate module.

The foot plate module consists of the foot plate and a hex bar. The foot plate will need to have multiple places for the hex bar to load the torque. Torque is transmitted and measured using a torque wrench on the hex bar.

We needed to choose a hex bar that would not shear with the rotational torque of 10 Nm. Modeling the hex bar as a shaft with a circular cross section, we used the shear stress equation (8):

$$\tau = \frac{T \cdot r}{J}$$

Where T is the applied torque, r is the radius of the hex bar, and J is the polar moment of inertia. The calculated shear stress is 141.4 MPa. With the yield shear strength of the material, steel, being 400 MPa, we have a safety factor of 2.8.

We also calculated twist angle with the following equations (9) (10):

$$K = \frac{G \cdot J}{L} \qquad \phi = \frac{T}{K}$$

Where G is the shear modulus of 79 GPa and L is the length of the hex bar. We get a twist angle of 0.17 radians (9.74 degrees). The small twist angle ensures that there is minimal deformation and still sufficient torque transmission of torque to the cleat.

4.6 Angular Motion Bars

The angular motion bars shown in Figure 9 were created for the purpose of being able to change the angle of the vertical force module. This mimics the biomechanical motion of changing the angle between the knee and the foot, which is common during cutting movements in soccer. These bars allow the angle to be changed from 0 to 45 degrees. In order to change the angle, a person can unscrew the pins from the nut, change the angle of the vertical force module, and then screw the pins in place to lock the vertical force module in place.

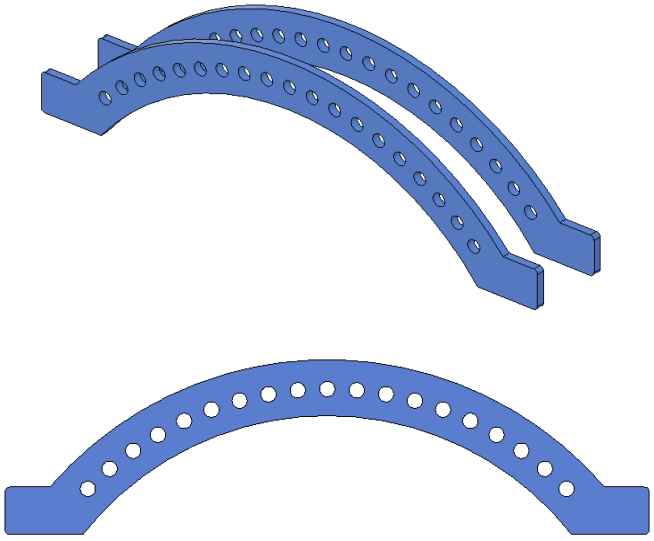

Figure 9: CAD model of the angular motion bars.

The angular motion bars determine the width of the base. The bars need to be a certain width because the vertical module pivots at the ankle joint, mimicking how the knee pivots along the ankle joint during a cutting movement. The distance from the ankle joint to the nut determines the radius of the curve in the angular motion bars. From here, the angle of 45 degrees determines the length of the bars.

In order to determine the thickness and height of the bars, an analysis on the maximum stress of the bars given different loading conditions was performed. In order to do a first order analysis, the curved bars were simplified to a straight bar with the same cross section as shown in figure 10. This is a conservative analysis since an arch will always be stronger than a straight bar.

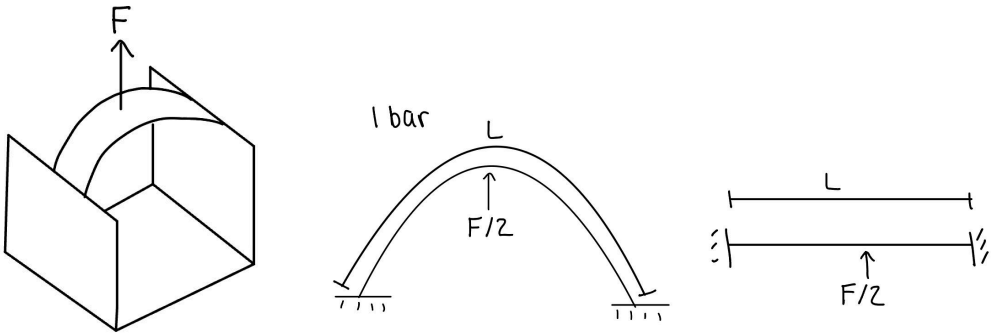

Figure 10: First order analysis of the curved bar with the vertical loading condition.

The first loading condition analyzed was the vertical loading condition, where all of the vertical force is applied at the center of the arch or beam. Since there are two bars, the force in the center is F/2, where F is the 2000 N force applied by the vertical force module. From here, the maximum moment on the beam and the maximum stress can be found as seen in figure 11.

$$M_{max} = \frac{FL}{8}$$

$$\sigma_{max} = \frac{M_{max} y}{I} = \frac{\frac{FL}{8}\frac{h}{2}}{\frac{th^3}{12}} = \frac{3FL}{4th^2}$$

Figure 11: Calculations of the maximum moment and maximum stress in the beam for the vertical condition are shown on the left and the cross section of the beam is shown on the right with height h and thickness t.

Next, an analysis of the angled loading condition is done as seen in figure 12 where an angle of 22.5 degrees is analyzed. Since this would be applied about 3/4L from the end of the arch, this condition is modeled as a simply supported beam with a force of F/2 applied 3/4L from the end of the bar. It is able to be modeled as a bar again for the first order analysis because an arch is stronger than a straight beam and the force is applied perpendicular to the arch at this point. The maximum moment is calculated followed by the maximum stress to give us information about how to size the thickness and height of the beam.

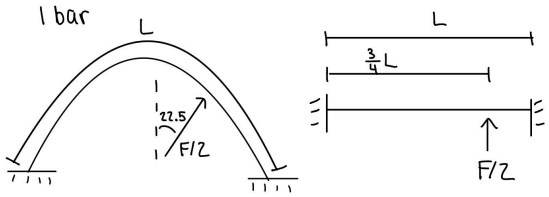

$$M_{max} = \frac{3FL}{32}$$

$$\sigma_{max} = \frac{M_{max} y}{I} = \frac{\frac{3FL}{32}\frac{h}{2}}{\frac{th^3}{12}} = \frac{9FL}{16th^2}$$

Figure 12: Calculations of the maximum moment and maximum stress in the beam for the angled loading condition of 22.5 degrees.

In order to achieve a high yield stress we chose the material Aluminum 6061-T6 and chose the cross section to have dimensions of 1 cm (thickness) x 4.87 cm (height). This gives us a maximum stress of 43.9 MPa for the vertical loading condition and a max stress of 33.0 MPa for the angled loading condition. Since Aluminum 6061 has a yield stress of 276 MPa, this part has a stress safety factor of greater than 6, which is sufficient for the purpose of this design.

4.7 Base

The base of the system is composed of T-slotted framing rails connected with corner brackets as shown in figure 13. The bottom of the base is a square in order to allow full rotation of the shoe within the system. This is useful when switching between measuring translational traction forces and rotational tractional forces as well as when applying the torque. When the torque is applied, the cleat will need room to rotate within the base frame. The width was determined by the size of the angular motion bars to be 664.074 mm and the height was determined by the height of the vertical force module to be 335.52 mm. There are various sizes for the T-slotted framing rails, but we decided on the 40 mm x 40 mm hollow rails. We compared the maximum stress in every member of the base for hollow vs solid bars in order to make this decision.

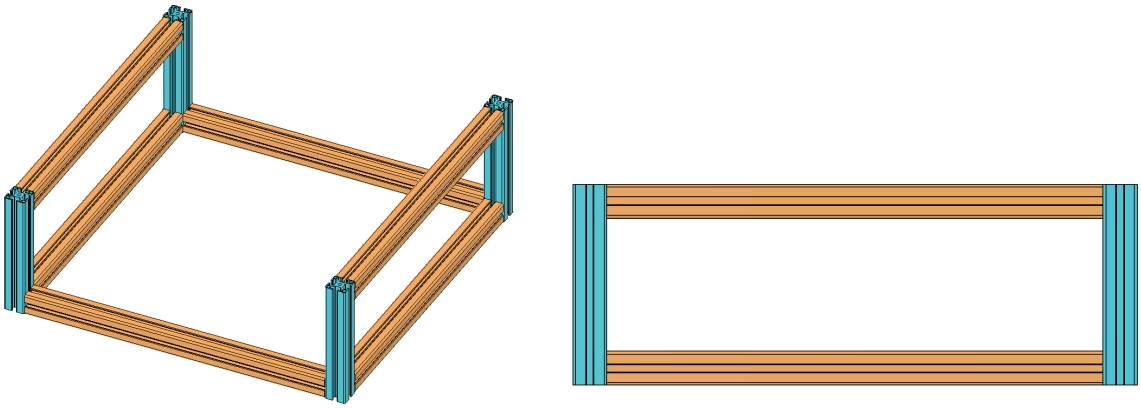

Figure 13: CAD of the base of the system. The horizontal bars are shown in orange and the vertical bars are shown in blue.

To start this analysis, the forces through the base must be traced with a structural loop. Figure 14 shows a structural loop of the entire system where the forces go from the vertical force module into the two angular motion bars. Each angular motion bar has a force of F/2 applied to it at the center of the bar. Only the vertical loading condition is analyzed since the angled loading condition produces a lower maximum stress as shown in the analysis of the angular motion bars above. The two top horizontal bars of the base shown in figure 15 in blue each have two forces of F/4 applied at a distance a apart in the middle of the bar. This distance a is the distance between the two angular motion bars. The force is then transferred to the vertical bars shown in figure 16, which each receive a force of F/4 from the top horizontal bars. The vertical bars then split the force between the 3 horizontal members with standing plates attached to them. This is because the members with standing plates attached to them are the ones that will have a person standing on them and therefore a reaction load to counteract the force generated from the system. The fourth horizontal bottom member does not receive any of this load. Each of the 3 horizontal members with standing plates shown in figure will experience a total force of F/3 from the vertical members, with F/6 on each end of the bar. This force will be counteracted by a force of F/3 from the hinges, which are attached to the standing plates. The force of F/3 will be split between the two attachment points on the hinges which are a distance of b apart, as seen in figure 17.

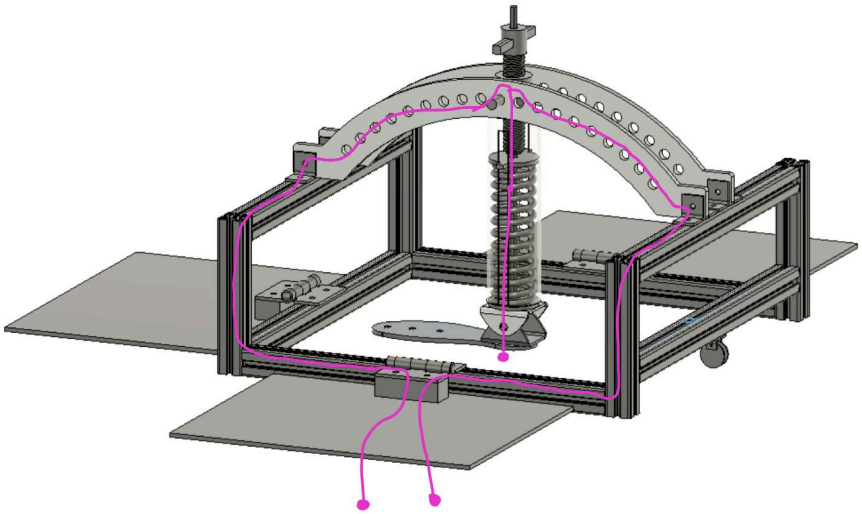

Figure 14: Structural loop through the whole system shown in pink. The loop is shown through the part facing us to make the diagram more clear, however the same loop is mirrored in the 2 other sides of the system with the standing plates as well.

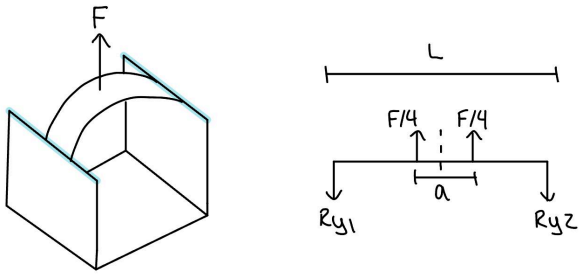

$$\sigma_{max} = \frac{M_{max} y}{I} = \frac{F(L-a)\frac{h}{2}}{8I}$$

Figure 15: Free body diagram of the top horizontal bars. The distance a represents the distance between the angular motion bars.

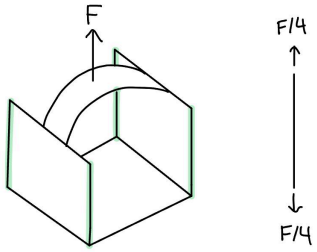

$$\sigma_{max} = \frac{Force}{Area} = \frac{F/_4}{A} = \frac{F}{4A}$$

Figure 16: Free body diagram of the 4 vertical bars with calculations for the maximum moment and maximum stress on each bar..

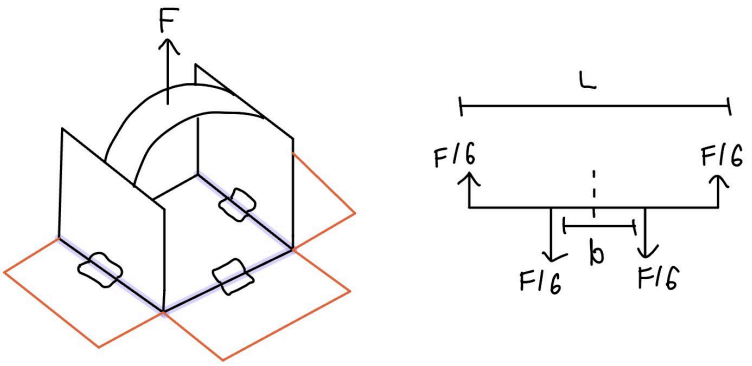

$$M_{max} = \frac{F(L-b)}{12}$$

$$\sigma_{max} = \frac{M_{max}y}{I} = \frac{F(L-b)\frac{h}{2}}{12I}$$

Figure 17: Free body diagram of the 3 horizontal bars that are attached to the standing plates with the calculation of the maximum moment and maximum stress in each bar. The distance b represents the distance between attachment points on the hinges.

Bar	Max Stress Hollow Rails (MPa)	Max Stress Solid Rails (MPa)
Top Horizontal	0.005	0.0036
Vertical	0.84	0.55
Bottom Horizontal	0.0036	0.0026

Figure 18: Results of the maximum stress on each member after plugging in the inertia of the hollow rails and solid rails to the formulas derived in figures 6-8.

After determining the formula for maximum stress in each of the bars, the inertia of a hollow rail and the inertia of a solid rail were plugged in to determine the maximum stress in each bar with a hollow vs solid rail profile. Since these bars are Aluminum and have a yield stress of 276 MPa, none of the stresses on the hollow rails as shown in figure 18 are concerning. Since the hollow rails are cheaper and lighter, we will use these for our design.

4.8 Standing Platforms and Hinges

The purpose of the standing platforms is for people to stand on them in order to clamp the system to the ground during the application of forces. The hinges are included so that the

standing platforms can be easily folded up after use, making the system portable. A single platform and hinge system is shown in figure 19.

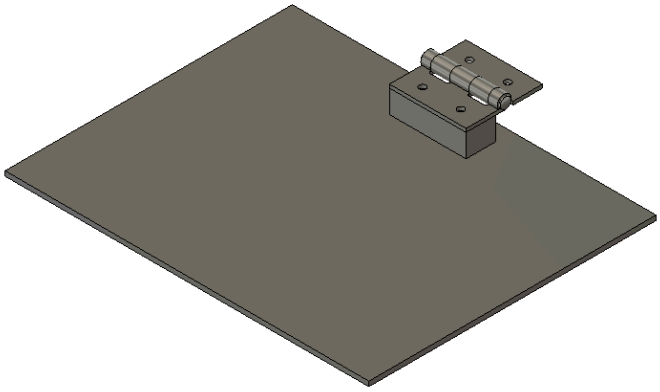

Figure 19: CAD of the standing plate and hinge system.

The main point of analysis here is the hinge, as that is the smallest member that will experience the greatest forces here. To analyze this, the 3 pieces of the hinge are split up and the reaction forces between them are determined as shown in figure 13. Since the rod is the thinnest member that is experiencing the most force, this is the part of most concern and is analyzed first. The maximum moment and maximum stress in the pin were calculated in figure 20, giving a maximum stress of 54.5 MPa. The pin is made of low-carbon steel which has a yield stress of 200 MPa. This results in a safety factor of 3.67 for this part, which is sufficient for the purpose of this system. The other two parts of the hinge are not analyzed as they have a much larger inertia than the rod with the same forces, resulting in lower stresses.

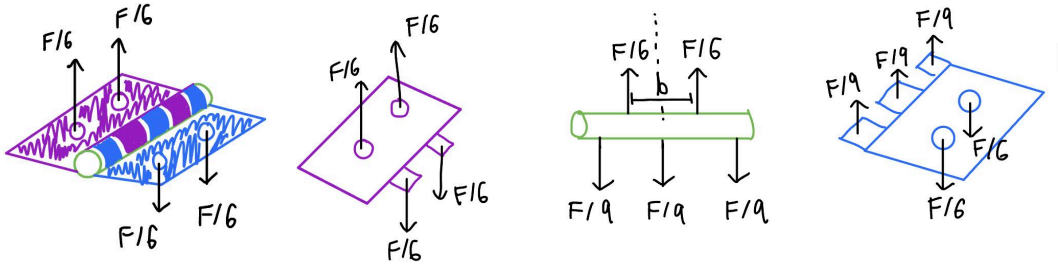

Figure 20: Free body diagram of the hinge and each of the 3 components that make up the hinge.

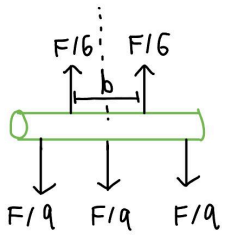

$$M_{max} = \frac{F(L-b)}{18}$$

$$\sigma_{max} = \frac{M_{max}y}{I} = \frac{\frac{F(L-b)}{18}\frac{D}{2}}{\frac{\pi D^4}{64}} = \frac{16F(L-b)}{9\pi D^3}$$

Figure 21: Free body diagram of the pin and calculations of the maximum moment and maximum stress on the pin.

To ensure that the forces were followed through the system correctly, we finish up the analysis with the base plate. The force on each plate should be F/3, allowing it to be secured by a 150lb person on each side. Figure 22 shows that this is consistent with the forces that we followed through the system as the base plate will have a force of F/3 from the rest of the system upwards, which the person can counteract with their weight.

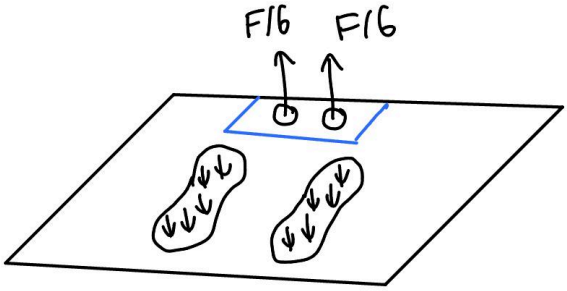

$$F_{person} = \frac{F}{3} = \frac{2000N}{3} = 667N = 150lbs$$

Figure 22: Free body diagram of the base plate with a person standing on it. The force needed by a person to keep the plate secured was calculated at 150lbs.

4.9 Horizontal Force Module

The horizontal force module will be a pulley system where there is a rope attached to the foot plate that runs horizontally, then around the pulley where the direction is changed to vertical. This allows a person to more easily be able to pull the rope without any errors in accuracy due to not pulling exactly horizontal. The horizontal force needed is 100N. We

originally thought this was doable for a single person, but after experimentation realize that we will need to modify this system slightly. The new design will feature multiple pulleys in a block and tackle type of system. Designing the details of this system will be one of our next steps. The current pulley system is pictured below in figure 23.

Figure 23: CAD of the pulley system on left and a diagram of how the pulley system interacts with the rest of the system shown on the right.

4. Design Improvements

As we iterate and go through the design review process, there are points of improvement for our device as we continue the project.

1. The angle of the vertical force might be difficult to adjust using the current design of the angular motion bars. In order to change the angle, the user needs to unscrew two pins, move the system, and rescrew the pins in. To fix this issue, we will redesign the angular motion bars to have a continuous movement system rather than a discrete movement system.
2. The pulley system for the horizontal module might be too difficult for one user to pull since the force needed is 100N. In order to fix this, we will add more pulleys in a block and tackle type of system. This will reduce the force needed by the user to pull 100N.
3. If one person steps off of the system while it is loaded, the system could flip onto another person since the hinge allows movement in this direction. To counteract this, we will use a hinge that locks into place at the bottom and that can be unlocked to fold up the system.
4. If one person steps off the system while it is loaded, the system may exert a force on the other two people, causing them to lift off of the ground. To ensure that this doesn't result in a dangerous scenario, we can make the compression distance of the spring less than one inch. In addition, to ensure that this will not damage the system, we could make sure the parts can withstand forces of up to 1000N.

5. The pin connecting the vertical force module to the angular motion bars does not have a sufficient safety factor. To decrease the stress on this part, we will replace it with a custom bearing piece that will span the distance between the angular motion bars and has two short cylinders extruding out each side which will attach it to the angular motion bars. This will also decrease the cost of the system since the previous bearing we used was one of the more expensive parts of the system.
6. The standing platforms will be costly if they are made of aluminum. To fix this, we will choose a cheaper material.

5. Conclusion

In moving forward, we will fix the design issues mentioned above by the start of IAP. We can then order the parts that we want so that we have them for the spring semester. There is a UROP student who will join us and will be here over IAP. He has offered to manufacture some of the parts that need machining. In the spring, we will put the system together and test it on the fields around MIT and the greater Boston and Cambridge area.

6. References

1. Boden, B. P., Griffin, L. Y., Garrett, W. E. Jr. (2000). Mechanisms of anterior cruciate ligament injury. *Orthopedics, 23* (6), 573–578.

2. Fong, C. M., Blackburn, J. T., Norcross, M. F., McGrath, M., & Padua, D. A. (2011). Ankle-dorsiflexion range of motion and landing biomechanics. *Journal of Athletic Training, 46* (1), 5–10.

3. Griffin, L. Y., Agel, J., Albohm, M. J., Arendt, E. A., Dick, R. W., Garrett, W. E., Garrick, J. G., Hewett, T. E., Huston, L., Ireland, M. L., Johnson, R. J., Kibler, W. B., Lephart, S., Lewis, J. L., Livingston, B., Malone, T. R., McCarty, E. C., & Wojtys, E. M. (2000). Noncontact anterior cruciate ligament injuries: Risk factors and prevention strategies. *Journal of the American Academy of Orthopaedic Surgeons, 8* (3), 141–150.

4. Griffin, L. Y., et al. (2006). Understanding and Preventing Noncontact ACL Injuries: A Review of the Hunt Valley II Meeting, January 2005. *American Journal of Sports Medicine.*
10. Hewett, T. E., Myer, G. D., Ford, K. R., et al. (2005). Biomechanical measures of neuromuscular control and valgus loading of the knee predict anterior cruciate ligament injury risk in female athletes: A prospective study. *The American Journal of Sports Medicine, 33* (4), 492–501.

5. Livesay, G. A., et al. (2006). "Cleated Shoes and Knee Joint Torques." *American Journal of Sports Medicine.*

6. Meyer, E. G., & Haut, R. C. (2008). Anterior cruciate ligament injury induced by internal tibial torsion or tibiofemoral compression. *Journal of Biomechanics, 41* (16), 3377–3383.

7. Orchard, J. (2001). "Is there a relationship between ground and climatic conditions and injuries in football?" *Sports Medicine.*